Computers in Industry 64 (2013) 1178–1185

Contents lists available at SciVerse ScienceDirect

Computers in Industry

journal homepage: www.elsevier.com/locate/compind

3D imaging application in the studies of micro air vehicles

Yanan Yu [a,*], Qingping Yang [b], Xiangjun Wang [c]

[a] School of Information Technology and Engineering, Tianjin University of Technology and Education, Tianjin, China
[b] School of Engineering and Design, Brunel University, London, UK
[c] MOEMS Education Ministry Key Laboratory, Tianjin University, Tianjin, China

ARTICLE INFO

Article history:
Received 30 August 2012
Received in revised form 19 May 2013
Accepted 5 June 2013
Available online 27 July 2013

Keywords:
3D stereo vision
Micro air vehicle (MAV)
Wind tunnel
Scale invariant feature transform (SIFT)
Model reconstruction
3D visualization

ABSTRACT

3D techniques are increasingly used in aerospace industry to improve quality and performance of aircrafts. This paper presents a 3D imaging technique for studying the aerodynamic shape and flight performance of micro air vehicles. 3D stereoscopic vision, based upon stroboscopic imaging, was utilized to obtain the 3D information of the aircraft's flexible aerodynamic surface. The aircraft models with deformable aerodynamic shape were designed and tested in a purpose-built wind tunnel experimental environment. After calculation of SIFT feature points and subdivision of triangular meshes, deformable surface of the aircraft's aerodynamic shape was represented. The aircraft's 3D visualization was used for analyzing unsteady deformation in the aerodynamic shape under external airflow disturbances. The results, together with aerodynamic forces measured in the experiment, will be useful to improve the flight performance and disturbance resistance ability of micro air vehicles.

1. Introduction

3D techniques and related products have found increasing applications in our life, e.g. 3D photo, film, television, camera as well as 3D animation. They have become the leading edge technology and trend in many industrial sectors. In engineering and manufacture industry, 3D techniques are also widely utilized, they have over the recent years advanced significantly and have been used to improve general product quality and production efficiency. Especially in some hazardous or inaccessible working areas, 3D imaging techniques have distinct practical utility for dimensional measurement, volumes measurement, or defect detection. The main 3D imaging techniques are laser triangulation, structured light, stereo vision, photogrammetry which are all based on triangulation, and time of flight, which depends on time delay [1].

In space industry and especially in aircraft testing, 3D imaging and visualization is usually an effective and intuitional way to be applied [2]. Micro air vehicle (MAV) is one branch of unmanned air vehicles [3]. Due to its small scale, quick response and low speed, the methods used to study aerodynamic characteristics and flight properties (including aerodynamic shape and pressure force) will be very different from traditional ones used for aircrafts. Common testing techniques for aerodynamic characteristics of micro air vehicles include contact sensor measurement [4], non-contact stereo visual measurement [5], smoke flow visualization measurement [6], and so on.

Inspired by bionics [7], a vertical take-off and landing micro air vehicle using flexible membrane structure as the aerodynamic shape was proposed in this paper. Due to its light weight and flexible properties, visual measurement and visualization techniques have significant advantages over contact measurement techniques. A 3D stereo vision testing method, based upon stroboscopic imaging technique, was used to obtain deformation produced in the MAV aerodynamic shape. Through a series of computation, reconstruction and representation, deformable aerodynamic membrane shape's 3D visualization was finally obtained. In order to characterize the impacts of aerodynamic force on the MAV model, the MAV model was simulated under certain turbulent air flow field in a wind tunnel experimental environment. The analysis about the relationship between the aerodynamic shape deformation and the flight performances will help researches to gain in-depth understanding of the MAV's characteristics. Subsequently, in design process, the flight performance and disturbance resistance ability of the MAV with flexible membrane will be improved. In Section 2, the theory of 3D imaging technique for morphology deformation of ducted-fan hovering MAV is presented. In Section 3, experimental conditions including aircraft prototype and test environment are described. In Section 4, the deformable aerodynamic membrane of the aircraft model is

* Corresponding author at: Room 1024, Building A, Tianjin University of Technology and Education, 1310 Dagu South Road, Hexi District, Tianjin 300222, China. Tel.: +86 13752430545.
E-mail address: jesuisyyn@hotmail.com (Y. Yu).

0166-3615/$ – see front matter © 2013 Elsevier B.V. All rights reserved.
http://dx.doi.org/10.1016/j.compind.2013.06.009

calculated and presented. The conclusions are then drawn in Section 5.

2. Theory

In the study, a vertical ducted-fan hovering MAV with flexible aerodynamic shape was designed and fabricated as the research object. The details will be presented in Section 3. In order to detect its morphology deformation and further to analyze its unsteady aerodynamic characteristics and flight performance, 3D stereoscopic vision based on stroboscopic imaging technique was used in the wind tunnel experimental environment. Spatial information of aircraft model's deformable surface was extracted using features' scale invariant characteristics and then directly represented using subdivision algorithm. The flow chart of the 3D imaging test algorithm is shown in Fig. 1, with each major stage of calculation discussed as follows.

2.1. 3D visualization method

For a high-speed moving object, high frame rate imaging devices are usually employed to observe its movement track as well as the attitude and morphological changes during its movement. In addition, a moving object with high speed could also be tracked and recorded in one frame image by using successive exposure approach. Different from the traditional test method using high quality equipment to record continuous images of a moving target, stroboscopic imaging approach presents continuous disturbance information of flexible aerodynamic shape in one image. The main advantage is not only avoiding the experimental requirement for high quality devices, but also providing a better visualization of object's whole motion and altitude variation.

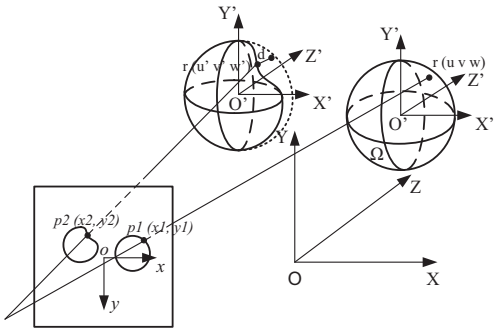

Fig. 2. Schematic stroboscopic imaging in a world coordinate system.

Stroboscopic imaging is a real-time recording technique. During one camera exposure time, optical integral is only produced in a short illumination time of strobe light on the CCD sensors. If illumination time is short enough, the position of high-speed moving object during this time is limited in a small rang to present instantaneously the state of this object. After each flash, optical integral is completed as there is no light output till next flash and the above process is then repeated. So after several cycles, there will be dozens of overlapping images of the moving object in different positions in one frame. Through adjusting the exposure time and the frequency of strobe light, this approach is able to detect aircraft aerodynamic shape and observe its transient changes intuitively. Given the same exposure time, the testing speed of the flying aircraft model partly depends on the frequency

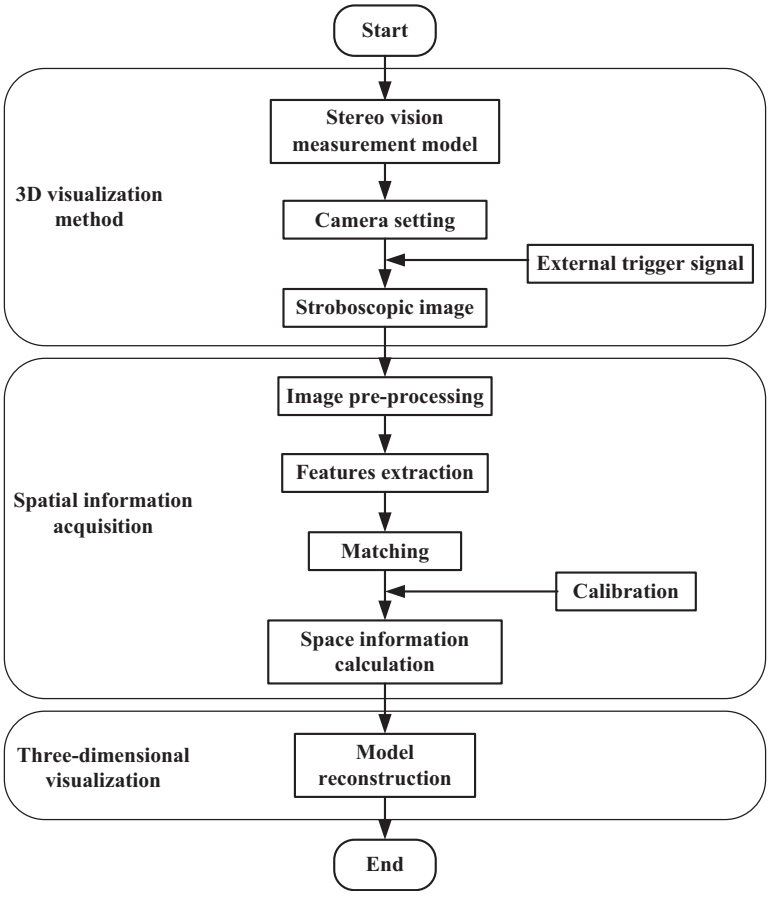

Fig. 1. Flow chart of 3D imaging test algorithm.

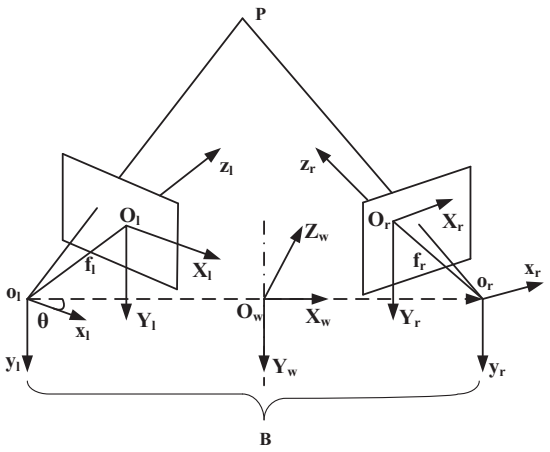

Fig. 3. The structural model of binocular vision measurement system.

of the strobe light. The schematic stroboscopic imaging in a world coordinate system is shown in Fig. 2.

For simplicity, Fig. 2 shows how two motion pictures of the moving object are recorded with stroboscopic image. *O-XYZ* is selected as the world coordinate system and *o-xy* is an image coordinate system. The transformation matrix between these two coordinate systems is composed of a rotation matrix *R* and a translation matrix *T*, which can be calculated by the Zhang's calibration method [8]. $r(u, v, w)$ refers to one point in the model coordinate system O'-$X'Y'Z'$, in which system the origin is at the centroid position of the MAV model Ω. The image coordinates of this point are $p_1(x_1, y_1)$. Due to the air pressure around the model, the flexible aerodynamic shape will produce a deformation and the location of the original point will change to $r(u', v', w')$. The image coordinates of this point also change to $p_2(x_2, y_2)$. So the positions at both flight moments and any changes produced in the aerodynamic shape are recorded in this image.

Stereo vision measurement model was used in the wind tunnel experimental environment, as shown in Fig. 3. Triangulation technique is the basis for stereo vision measurement model as two cameras and the tested object form a triangle. With the calibration results of the two cameras' intrinsic and extrinsic parameters, three dimensional information of any spatial point in the experimental environment can be calculated.

The effects of structural parameters on the system accuracy and error distribution are necessarily considered in the process of equipment installation. For example, system error is the smallest when baseline distance *B* is 1.3 times the working distance *z*; the changes of error distribution along the line on which the two angles between the optical axes and the baseline are equal is not obvious, and so on.

2.2. Spatial information acquisition

Information extraction tasks based on the stroboscopic image need to be completed to obtain the disturbance information on aircraft's aerodynamic shape, including image pre-processing, features extraction, and matching.

2.2.1. Image pre-processing

In order to improve reliability of the processing of the obtained images, image pre-processing step is an important part of the data mining process. Irrelevant data and noises need to be removed from the image while useful information needs to be recovered. The observability of image information should be enhanced to maximize the data. Usually pre-processing involves digitalization, geometric transformation, normalization, and image enhancement, etc. In this project, image pixel normalization in the acquired stroboscopic images was performed, and the intensity value of gradation histogram was linearly expanded to remove noise and increase the image contrast.

2.2.2. Feature extraction

During image acquisition process, the scale space of images varies with object movement. There are also some changes in illumination due to the successive exposure. Compared with other feature extraction methods such as SUSAN, Harris and Harris–Laplace, Scale Invariant Feature Transform (SIFT) feature points are more suitable for images with scaling, rotation, noises and partial changes in local deformation and illumination [9]. In addition, SIFT features are convenient and quick to be matched with different image features [10] as they have robust feature descriptors. In the meantime, invariant key points from 2D image can be used in retrieving similar models in 3D models database [11].

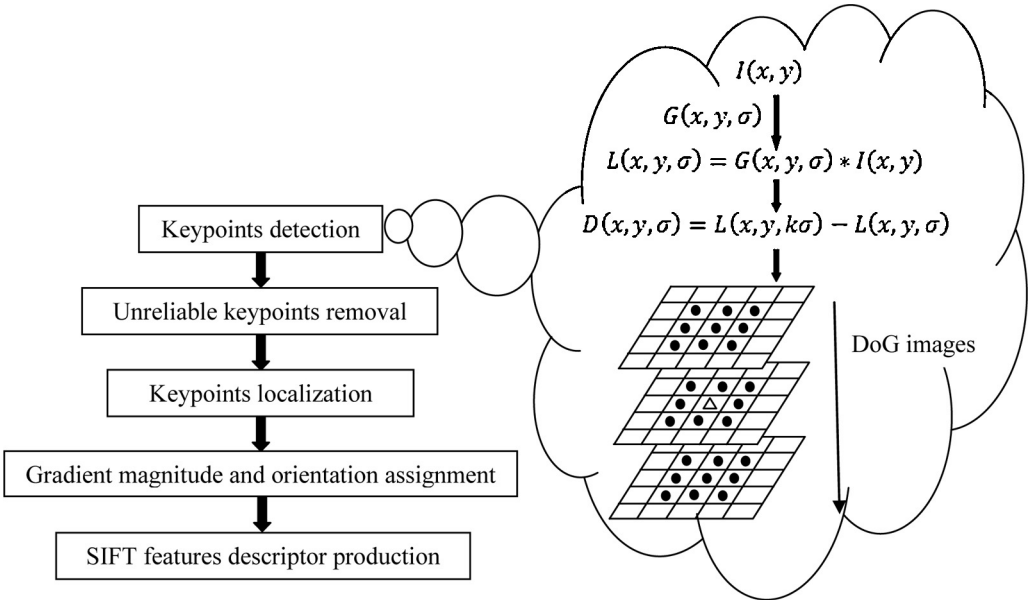

Fig. 4. Flow chart of SIFT algorithm.

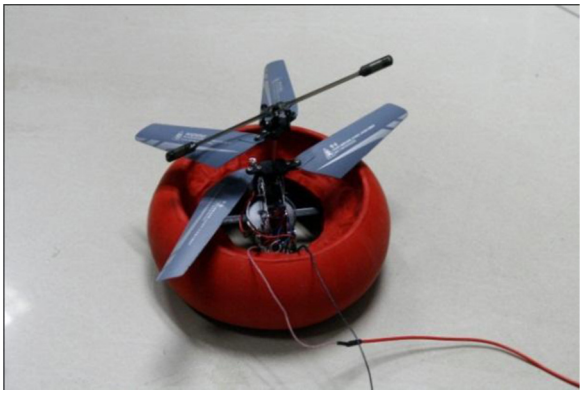

Fig. 5. Experimental prototype with flexible aerodynamic shape.

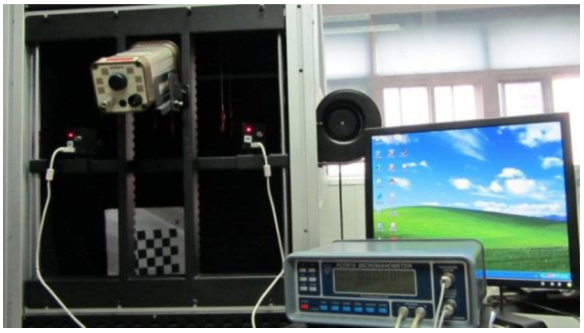

Fig. 6. Wind tunnel experimental system.

For the stroboscopic images containing the aircraft model's movement and the elastic deformation in its aerodynamic shape, a SIFT algorithm was employed to extract features from the texture on the surface. The flow chart of the SIFT algorithm is presented in Fig. 4.

2.2.2.1. Scale space keypoints detection. The scale space of an image, $L(x, y, \sigma)$, is constructed from the convolution of a variable-scale Gaussian, $G(x, y, \sigma)$, with an input image, $I(x, y)$, as:

$$L(x,y,\sigma) = G(x,y,\sigma) \times I(x,y) \tag{1}$$

where $G(x, y, \sigma)$ is a variable-scale Gaussian kernel

$$G(x,y,\sigma) = \frac{1}{2\pi\sigma^2} e^{-(x^2+y^2)/2\sigma^2} \tag{2}$$

Scale space keypoints are detected from difference-of-Gaussian images, $D(x, y, \sigma)$, which is computed from the difference of two nearby scale space images:

$$\begin{aligned} D(x,y,\sigma) &= L(x,y,k\sigma) - L(x,y,\sigma) \\ &= (G(x,y,k\sigma) - G(x,y,\sigma)) \times I(x,y) \end{aligned} \tag{3}$$

On each difference-of-Gaussian image, the extrema are detected by comparing each pixel with its 26 neighbors in 3×3 regions at its scale and two adjacent scales, shown in Fig. 4. The extrema as candidate features involve maxima and minima.

2.2.2.2. Keypoints localization. Because some interest points have low contrast and some are ambiguous on the boundary, the threshold parameters are defined for the evaluation of each candidate feature. After eliminating false features, accurate location information of each SIFT feature is recorded in the database.

2.2.2.3. Orientation assignment. Schiele and Crowley proposed the use of multidimensional histograms to represent the distribution of features within image regions [12]. This type of feature is also particularly useful for recognition of textured objects with flexible deformable shapes.

The gradient magnitude, $m(x, y)$, and orientation, $\theta(x, y)$, at each pixel of the image region can be respectively calculated to construct eight directions weighted histogram:

$$\begin{aligned} m(x,y) &= \sqrt{f_x(x,y)^2 + f_y(x,y)^2} \\ &= \sqrt{(L(x+1,y) - L(x-1,y))^2 + (L(x,y+1) - L(x,y-1))^2} \end{aligned} \tag{4}$$

$$\theta(x,y) = \arctan\frac{f_y(x,y)}{f_x(x,y)} = \arctan\frac{L(x,y+1) - L(x,y-1)}{L(x+1,y) - L(x-1,y)} \tag{5}$$

2.2.2.4. Descriptor production. To describe feature and its surroundings, a unique descriptor is calculated. The descriptor is created by computing the gradient magnitude and orientation of each sample point in a region around the keypoint location. In the actual algorithm, a 128 element feature vector is used for each keypoint.

2.2.3. Matching

Matching is adopted to find the same feature in aircraft aerodynamic shape among different locations in stroboscopic image. In order to improve the reliability of matching, for each feature, comparing the distance of the closest neighbor with that of the second-closest one is determined as the method of matching. For example, in the destination area P_{SIFT1} and P_{SIFT2} are the first two nearest feature points from keypoint P_{SIFT} in template area within Euclidean distance $Dist_1 = ||P_{SIFT} - P_{SIFT1}||$ and $Dist_2 = ||P_{SIFT} - P_{SIFT2}||$. The ratio of the nearest distance and the second-nearest distance is computed by Eq. (6).

$$T = \frac{Dist_1}{Dist_2} \tag{6}$$

(a) Histogram of left camera image (b) The image after contrast increasing

Fig. 7. Stroboscopic image obtained from left side camera.

(a) Histogram of right camera image (b) The image after contrast increasing

Fig. 8. Stroboscopic image obtained from right side camera.

If ratio T is less than threshold value ρ ($\rho = 0.8$ is an empirical value), SIFT feature P_{SIFT} in template area and P_{SIFT1} in destination area are determined as a correct matched pair.

2.3. Model reconstruction

Model reconstruction and 3D visualization based upon the experimental data can help researchers study geometric characteristics and physical properties. In order to determine and represent the deformable aerodynamic shape from the stereoscopic vision testing, the algorithm of subdivision surface has been used for solving surface fitting problem, i.e. generating the right surface from data points. More specifically it is based upon triangular mesh subdivision, an iterative process with each step mainly composed of splitting and positioning [13].

A triangular mesh is a regular mesh if all its vertices have a valence of six (valence refers to the number of vertices in the neighborhood of the vertex concerned). In a regular mesh, the position p' of the original vertex after new vertices inserted on the edges which connect with this vertex is located by Eq. (7):

$$p' = \frac{10}{16}p + \frac{6}{16}q \tag{7}$$

where p is the vertex's original position and q is the average position of nearby vertices which share edges with this vertex.

(a) Left camera image

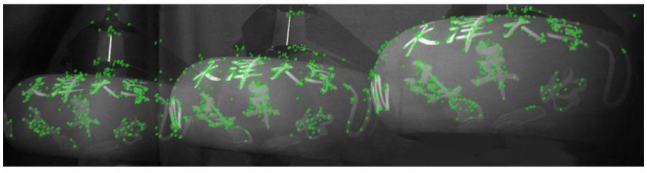

(b) Right camera image

Fig. 9. SIFT feature points extracted from stroboscopic images.

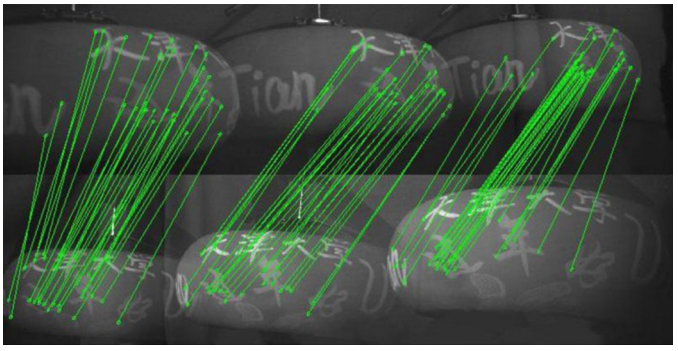

Fig. 10. Matched pairs between two stroboscopic images.

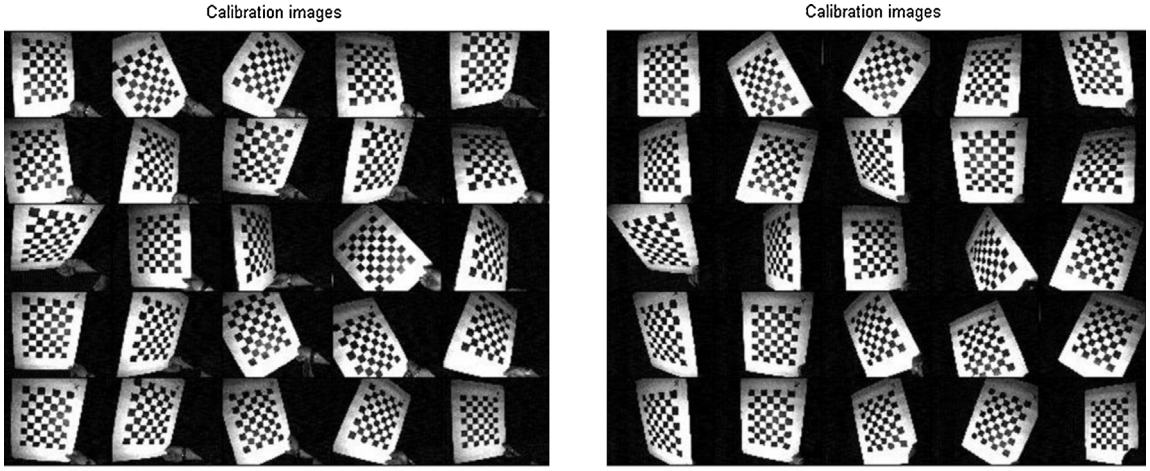

(a) Calibration images from left camera (b) Calibration images from right camera

Fig. 11. Calibration images of a planar checkerboard.

A vertex whose valence is not six is called an extraordinary vertex. For an extraordinary vertex, its new position is located by Eq. (8) [13]:

$$p' = (1 - k\beta)\,p + \beta(p_1 + p_2 + \cdots + p_k) \tag{8}$$

where p is the vertex's original position, p_i are positions of nearby vertices, k is the valence (i.e. number of nearby vertices), and coefficient β is calculated by Eq. (9):

$$\beta = \begin{cases} \dfrac{3}{16} & (k = 3) \\ \dfrac{1}{k}\left(\dfrac{5}{8} - \left(\dfrac{3}{8} + \dfrac{1}{4}\cos\dfrac{2\pi}{k}\right)^2\right) & (k > 3) \end{cases} \tag{9}$$

Using the method of subdivision described above, the initial triangular mesh can converge to a smooth surface after several iterations and repeated computing.

3. Experiment

The aircraft prototype designed in this study is a vertical ducted-fan hovering micro air vehicle. The elastic membrane structure surrounding the aircraft is deformable under an external airflow pressure. According to the results of orthogonal experimental design optimization completed in our previous work, the vertical duct and flexible membrane structure of experimental prototype were manufactured and assembled. Vertical duct component was machined by rapid prototyping machine and assembled. Because there are some holes on the duct wall for mass reduction, PE film was wrapped around it. Outside the PE film, rubber membrane was fixed on both the top and bottom edge of the duct wall to yield a closed circular air bag within the PE film. The air pressure of the internal space is consistent. An air hole is prearranged near side of the closed circular air bag for inflation and deflation. Twin screw and steering gear were installed on parallel bracket inside the duct to ensure that the center axis of lifting system coincides with the axis of vertical duct. The experimental prototype is shown in Fig. 5. The basic flight test was completed which showed that the aircraft model has a stabilized flight and good performance. In order to clearly inspect each point on the membrane structure of aircraft when using SIFT extraction algorithm, random texture or reference markings on the shape are necessary.

To study the MAV disturbance resistance ability and the 3D visualization method proposed above, a shading closed-loop experimental environment was established with a stroboscopic light, a photogrammetric instrument, an airflow generator, an air volume sensor, and the data acquisition and post-processing system, as shown in Fig. 6.

The wind tunnel test section has a 600 mm^3 space with a height adjustable frame construction. Air-permeable lightproof metal plates were employed around the space to reduce the influence of environmental factors. For convenient installation of various equipment and devices in the future, some sliding blocks are pre-installed along the top beam and the main support pillar of the test section.

An air blower with continuously variable transmission is used as airflow generator in the wind tunnel. It is able to simulate complicated vertical and horizontal turbulent air flow field. The type of air blower is 2GRE25 140 × 59R from ECOFIT France, with a 48 V external power supply, 0–10 V adjusting speed, 3200 RPM maximum rotational speed, and 600 m^3/h maximum output flow.

A multi-function transducer module used in the wind tunnel is FCO510 micro-manometer from Furness Controls UK. It assembles several sensors such as temperature, absolute air pressure (AP) and differential pressure (DP), and flowrate as well as air velocity. The measurement range of DP is 0–20 kPa and air velocity measurement range is 0–180 m/s. Pitot tube is used to measure the average flowrate in tunnel, by which differential pressure measured is a square function of air velocity. So the calculation of air velocity can be presented as the following formula.

$$V = 1.277\sqrt{\frac{H}{K} \times \frac{1.013}{P} \times \frac{T}{288} \times \frac{1}{\rho}} \tag{10}$$

where H is the differential pressure in Pa, T is the environmental temperature in K, P is the absolute pressure in Bar (1Bar = 105 Pa), ρ is the relative density, V is the air velocity in m/s, K is the factor of pitot tube.

Based on the measurement method mentioned above, the type of strobe light used is DT-311 stroboscope. Its flashing range is in 40–35,000 fpm (flashes per minute) with accuracy ±0.01% of reading. In order to have a relative stable airflow distribution in the wind tunnel, a real-time measurement of the airflow generator output value needs to be accomplished by micro-manometer to form a closed-loop control system.

4. Results and discussion

Synchronous external trigger mode of two cameras was selected which is single frame acquisition with 1 s exposure time. The cameras begin image acquisition with a falling edge trigger signal. According to the method mentioned in Section 2.2.1, the gradation histograms of the stroboscopic images from the left side and right side cameras and the images after contrast increasing are respectively shown in Figs. 7 and 8. Feature extraction results showed that texture information is increased after image enhancement.

In the process of SIFT features extraction, the scale space of input images were constructed first. Each pixel on different scale of image was compared with its neighbors and the extrema were extracted as the keypoints. After removing unreliable keypoints, there are 977 SIFT feature points in the left camera image and 1338 in right side as shown in Fig. 9. In each stroboscopic image, three locations of the aircraft model during its movement were recorded.

Using the matching method proposed in Section 2, the relationship of SIFT features at each location between two images were founded and constructed. Parts of the incorrect matches were discarded by comparing the distance of the closest neighbor with that of the second-closest one. However, some incorrect matches are still existent. In order to improve the accuracy of feature point matching, RANSAC algorithm was used to remove outliers. Final matching relationship between two stroboscopic images which shown in Fig. 10.

To calculate the three-dimensional coordinates of the SIFT feature points extracted and furthermore to reconstruct a world model of the membrane surface, the intrinsic and extrinsic parameters of the two cameras are necessary. The calibration method in this paper used Camera Calibration Toolbox for Matlab. 25 images of a planar checkerboard from each camera are acquired and computed, which are shown in Fig. 11.

Through stereo vision calibration, intrinsic and extrinsic parameters of stereo vision system were computed. Using related formulas and calibration results, three-dimensional coordinates of all extracted features in the world coordinate system could be calculated. For each location during object movement, the space coordinates of the extracted SIFT features contain the 3D information and morphology deformation of the aircraft flexible aerodynamic shape. In order to realize deformable surface reconstruction and visualization, an appropriate surface fitting algorithm is needed. As mentioned above, the triangular mesh subdivision algorithm was used to represent the 3D data extracted

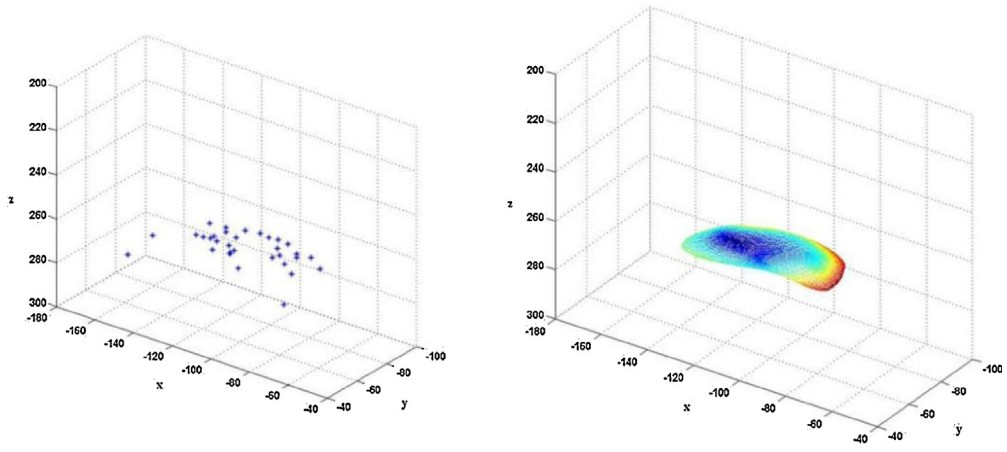

(a) First location from the left side

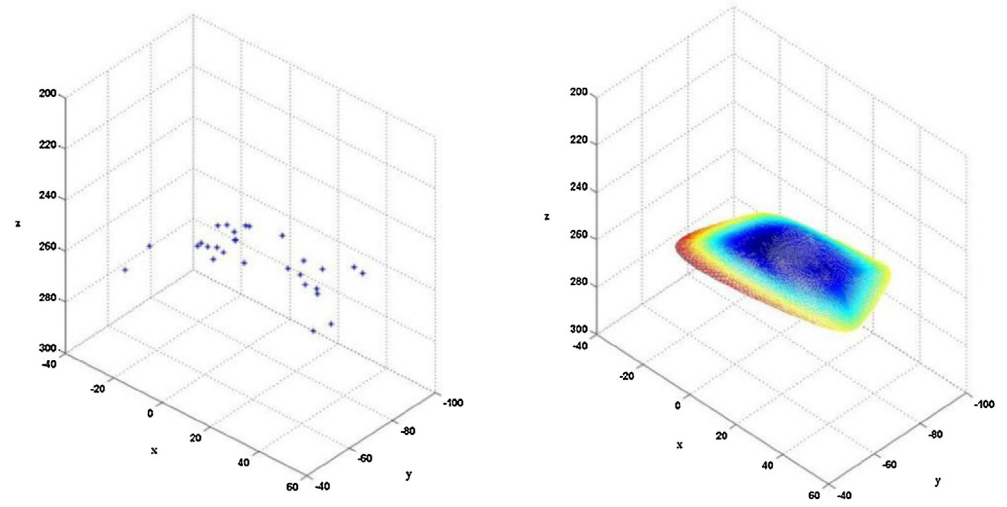

(b) Second location from the left side

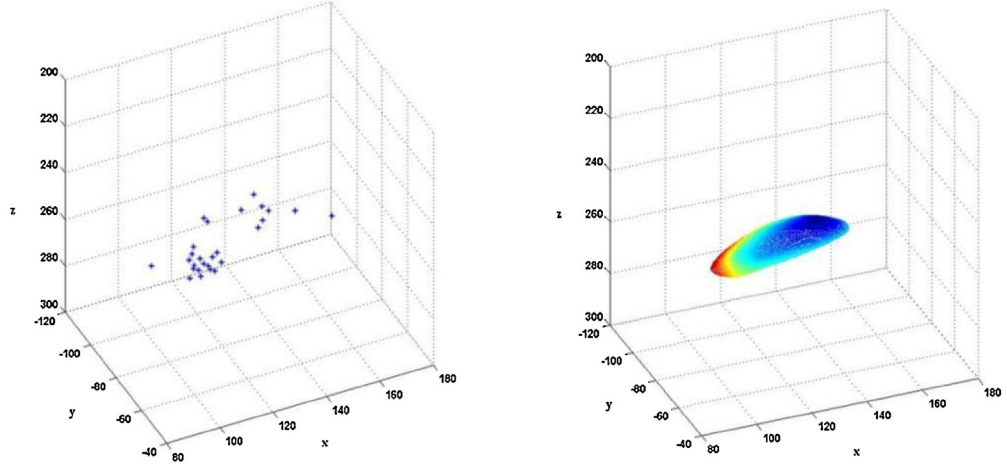

(c) Third location from the left side

Fig. 12. Subdivision results at three adjacent locations.

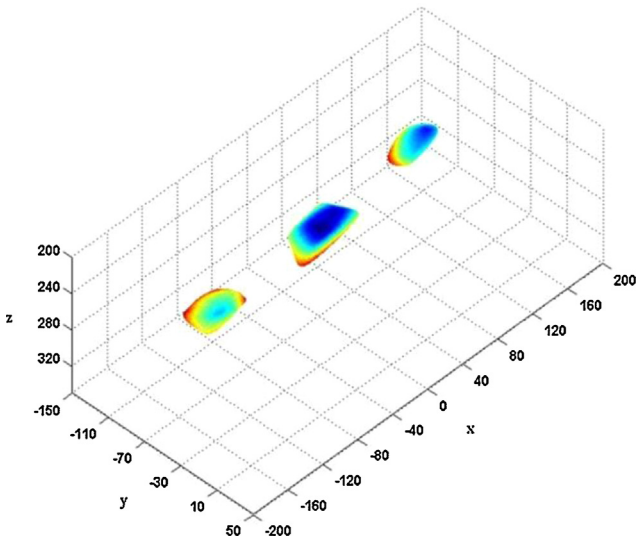

Fig. 13. Surface subdivision results based on 3D SIFT features.

Table 1
Morphology deformation of the membrane structure.

Location	Maximum deformation (mm)
First	2.93
Second	2.9
Third	0.84

from the membrane surface, which is able to obtain relatively smooth surfaces with fast computation. In Fig. 12, (a)–(c) represent SIFT feature space distributions and subdivision surface at three adjacent locations of the moving object respectively. The color of each smooth surface represents the depth information (in z axle) of triangular mesh in its coordinate system.

Typical result is shown in Fig. 13, which represents three adjacent location images of the moving object. The origin of world coordinate system is located at the center of baseline. The color of three triangular meshes represents the depth information (in z axle) in the world coordinate system.

In Fig. 13, each reconstructed surface is composed of two independent parts. One part is the variation of the aircraft's position, which is caused by the movement of its center of mass. The other part is the morphology deformation, which is caused by the air pressure on its membrane structure. At each location, the maximum deformation can be determined by calculating the distance between centroid and subdivision surface, which result is presented in Table 1.

From Fig. 13, only partial reconstructed surface of the vehicle which faces to the stereo vision system was built based on the experimental results. In the next research work, the whole 3D model of the aircraft will be studied and estimated to improve the quality of the test and flight performance of the vehicle.

5. Conclusions

In order to analyze flight stability and disturbance resistance ability of micro air vehicles, 3D detection and imaging has been used to study the movement of an aircraft model and the deformation produced in the aerodynamic shape when the object undergoes an external airflow pressure. Based upon stroboscopic imaging technique, stereoscopic visual measurements were performed to record continuous movement of the object and obtain 3D information of its surface. Triangular mesh subdivision algorithm was applied to represent the deformable surface smoothly. The results indicated that 3D detection method presented in this paper is effective and useful for analyzing aerodynamic characteristics and unsteady deformation of micro air vehicles with flexible membrane structure.

References

[1] G. Sansoni, M. Trebeschi, F. Docchio, State-of-the-art and applications of 3D imaging sensors in industry, cultural heritage, medicine, and criminal investigation, Sensors 9 (2009) 568–601.
[2] R. Albertani, B. Stanford, J.P. Hubner, P.G. Ifju, Aerodynamic coefficients and deformation measurements on flexible micro air vehicle wings, Experimental Mechanics 47 (2007) 625–635.
[3] B.-J. Tsai, Y.-C. Fu, Design and aerodynamic analysis of a flapping-wing micro aerial vehicle, Aerospace Science and Technology 13 (October–November) (2009) 383–392.
[4] D. Watman, T. Furukawa, A visualization system for analysis of micro aerial vehicle scaled flapping wings, Journal Intelligent and Robotic System 51 (2008) 369–381.
[5] Z.A. Khan, S.K. Agrawal, Optimal hovering kinematics of flapping wings for micro air vehicle, AIAA Journal 49 (2011) 257–268.
[6] S. Ho, H. Nassel, N. Pornsinsirirak, Y.-C. Tai, C.-M. Ho, Unsteady aerodynamics flow control for flapping wing flyers, Progress in Aerospace Sciences 39 (2003) 635–681.
[7] H. Aono, S.K. Chimakurthi, C.E.S. Cesnik, H. Liu, W. Shyy, Computational modeling of spanwise flexibility effects on flapping wing aerodynamics, in: 47th AIAA Aerospace Sciences Meeting including The New Horizons Forum and Aerospace Exposition, 2009, 1–18.
[8] Z. Zhang, A flexible new technique for camera calibration, IEEE Transaction on Pattern Analysis and Machine Intelligence 22 (2000) 1330–1334.
[9] D.G. Lowe, Distinctive image features from scale-invariant keypoints, Journal of Computer Vision 60 (2004) 91–110.
[10] T.-W.R. Lo, J.P. Siebert, Local feature extraction and matching on range images: 2.5D SIFT, Computer Vision and Image Understanding 113 (2009) 1235–1250.
[11] K.P. Zhu, Y.S. Wong, W.F. Lu, H.T. Loh, 3D CAD model matching from 2D local invariant features, Computers in Industry 61 (2010) 432–439.
[12] B. Schiele, J.L. Crowley, Recognition without correspondence using multidimensional receptive field histograms, International Journal of Computer Vision 36 (2000) 31–50.
[13] H. Suzuki, S. Takeuchi, T. Kanai, Subdivision surface fitting to a range of points, in: Proceedings of the 7th Pacific Conference on Computer Graphics and Applications, 1999.

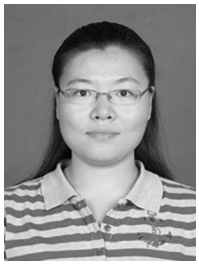

Yanan Yu received her PhD degree in precision measurement technology and instruments from Tianjin University in January 2013. From December 2010 to February 2012 she studied as an exchange PhD student in Brunel University, which was sponsored by Chinese government through the China Scholarship Council Postgraduate Scholarship. She is currently a lecture in Tianjin University of Technology and Education and her research interests include computer control technology, photoelectric detection and visual measurement.

Qingping Yang received his PhD in 3D dimensional metrology from Brunel University in 1992. He is currently a lecturer and the director of the Innovative Quality, Measurement and Smart Systems research group at Brunel University. His current research interests include advanced sensors, dimensional metrology, quality engineering, measurement science and smart systems. He has published more than 75 papers in these areas.

Xiangjun Wang received his PhD degree in precision measurement technology and instruments from Tianjin University. His current research interests include photoelectric sensor and testing, computer vision and image analysis, MOEMS and MEMS.